Increasing atmospheric dryness reduces boreal forest tree growth

Ariane Mirabel (ariane.mirabel@gmail.com)
University of Western Ontario https://orcid.org/0000-0002-7081-9922
Martin P. Girardin
Natural Resources Canada, Canadian Forest Service, Laurentian Forestry Centre
Juha Metsaranta
Northern Forestry Centre, Canada
Danielle Way
Australian National University
Peter B Reich
University of Minnesota, St. Paul https://orcid.org/0000-0003-4424-662X

Article

Keywords:

Posted Date: February 22nd, 2023

DOI: https://doi.org/10.21203/rs.3.rs-2611306/v1

Abstract

Rising atmospheric vapor pressure deficit (VPD) associated with climate change impacts tree growth and carbon storage through its effects on stomatal closure, evapotranspiration, and soil dryness. However, ground truth analyses of the effects of changing VPD on forest growth remain limited to focal species and areas. We assessed the response of Canada's boreal forests to VPD changes during 1951-2018 using a tree-growth increment network with 5,000 species-site combinations. Roughly half of the sites showed a relationship between growth and VPD, with the most common response being a negative relationship between previous year VPD and current year growth, while current year VPD also tended to reduce growth. Species, tree age and soil moisture were primary determinants of tree VPD responses, with younger trees and key species like Picea glauca and Populus tremuloides showing higher VPD sensitivity. Since 1951, increases in summer VPD in Canada have paralleled growth decreases, particularly in spruce species.

Introduction

Land carbon storage capacity varies across Canada's boreal forest due to local and regional differences in climate, vegetation, soils, surficial geology, and disturbance regime (Brandt et al., 2013). Climate change will alter this capacity because the Canadian boreal forest is dominated by cold-tolerant species and is warming faster than most other land areas (0.2˚C to 0.5˚C per decade over 1961–2015, Vincent et al., 2018; IPCC 2021). Warming is expected to alter the net annual carbon uptake of Canadian boreal forests, through changes to temperature-related variables (growing season length, drought severity, vapour pressure deficit, freeze frequency) that affect tree mortality, recruitment, physiology and growth (Boucher et al., 2018; Serreze et al., 2000; Hammond et al., 2022). The complexity of the boreal environment and diversity of boreal species produce notable contrasts in productivity responses to warming (Brandt et al., 2013; Pau et al., 2022; Reich et al., 2022). Across boreal Canada, forest productivity is anticipated to decrease in the west because of water stress, and increase north-eastward where temperature is currently the main factor limiting tree growth (Price et al., 2013; Girardin et al., 2016a; Wulder et al., 2020). Additionally, differential trajectories among tree genera, species and ecoclines are possible, depending on their stress tolerances and plasticity (Aubin et al., 2018; de Cárcer et al., 2018; Girardin et al., 2021a; Sánchez-Pinillos et al., 2019).

Atmospheric vapour pressure deficit (VPD), the difference between the concurrent amount of water vapour in the atmosphere and the potential amount held at saturation (López et al., 2021), is a major temperature-related determinant of plant physiology. Without a corresponding increase in the actual amount of atmospheric water vapour, VPD will increase with warming because the saturation vapour pressure is a curvilinear function of air temperature (Grossiord et al., 2020). High VPD can induce high leaf and soil water loss, increasing the risk of plant water deficits and stress (Denissen et al., 2022; Yuan et al., 2019). Water deficits increase xylem tension and tissue cavitation: these negative effects are minimized by stomatal closure, which decreases water loss at the cost of carbon uptake, leading to growth reductions and eventually tree mortality (Novick et al., 2016; Reich et al., 2018; Grossiord et al., 2020; López et al., 2021). Warming can thus enhance plant growth in cool and wet environments, but impair it above a threshold of water stress (Pau et al., 2022; Danneyrolles et al., 2022). From a hydrometeorological perspective, higher atmospheric dryness also increases atmospheric demand for water from the land surface, increasing evaporation and reducing available soil moisture (Lu et al., 2022). Hence, plant growth responses to atmospheric dryness can result from direct effects on stomatal conductance and indirect effects on soil moisture through increasing evapotranspiration (Zhang et al., 2019).

Tree species have evolved different strategies to cope with atmospheric dryness and differential responses to VPD changes, modulated by the environmental conditions (López et al., 2021). There is thus a need for in-situ, multi-species

comparisons to quantify these differences across a broad range of environmental conditions (Peng et al., 2011; Reich et al., 2018). Recent remote sensing studies have produced mixed results about the relative role of VPD on productivity and carbon uptake (Liu et al., 2020; Lu et al., 2022). Tree-ring studies offer an important opportunity to understand VPD impacts, especially pertaining to aboveground carbon uptake. To date, tree-ring analyses directly linking changes in dryness with boreal forest growth have focused on only a few species and areas (Babst et al., 2019). Integrating tree-ring sampling into national forest inventories has enabled large-scale ecological assessments related to forest health and carbon cycling, including in Canada (Girardin et al., 2021b; Evans et al., 2022). Quantifying large-scale tree growth response to VPD would improve our understanding of forest growth responses under climate change, and reduce uncertainties in the model predictions used to evaluate strategies for mitigating and adapting to climate change.

Here, we assess boreal forest responses to changes in atmospheric VPD using a well-replicated tree-ring network covering Canada's forests over the period 1951–2018. Using mixed-effects models, we quantified annual growth changes as a function of atmospheric VPD of the prior and current year of tree-ring formation. The growth-VPD relationships enabled mapping of spatially-explicit VPD responses across Canada's boreal zone. We then explored the main drivers of differential growth responses to VPD, including species, local precipitation and temperature, elevation, and tree age and size. Finally, we determined how VPD and growth are changing over time for the most responsive species.

Results

Forest response to atmospheric vapour pressure deficit

Among the 4,931 species-by-site additive mixed models (GAMM), 47% showed a significant relationship between annual basal area increment (BAI) and VPD across the nine species analyzed (*Picea mariana, Picea glauca, Pinus banksiana, Populus tremuloides, Pinus contorta, Pseudotsuga menziesii, Picea engelmannii, Abies lasiocarpa*, and *Pinus resinosa*). The average goodness-of-fit between year-to-year observed growth fluctuations and growth predicted from site-specific growth-VPD models was $r^2 = 0.51$ ($\sigma \pm 0.21$, $n = 4{,}931$ GAMM).

Among the species-by-site GAMM models, 22% (1,096 models) had a *t*-value for the relationship between annual BAI and VPD of the year of ring formation (VPD_t) achieving the $p < 0.05$ threshold. Of these 1,096 significant relationships, 752 (about two-thirds) were negative, indicating that increasing VPD_t is detrimental to tree growth for these sites-species combination (Fig. 2, Table 1). The majority of negative *t*-values were found near warm, dry margins of the boreal forest in southcentral Canada (*i.e.* southern part of the Boreal Shield ecoregion), specifically for *Picea glauca* and *Picea mariana* (Fig. 2). A third of the significant BAI-VPD_t *t*-value were positive (344 models), indicating that increasing VPD_t was positively related with current year tree growth (Fig. 2, Table 1). The positive *t*-values were found in western Canada, *i.e.* Boreal Cordillera, and in cooler moister areas of central and eastern Canada, *i.e.* Hudson Plain and Taiga Shield. Both negative and positive *t*-values were found for all species except *Pseudotsuga menziesii*, but its distribution area does not overlap the previously cited ecoregions. Additionally, 37% of the species-by-site GAMM models (1,659 models) showed a significant relationship with VPD of the year prior to ring formation (VPD_{t-1}), with a negative *t*-value for virtually all models (96%, Fig. 2), indicating that increasing VPD_{t-1} is detrimental to tree growth in these site-species combination. The consistency of the results was maintained in the partial BAI-VPD GAMM models, which aimed at controlling for the impact of summer soil moisture index (SMI) on growth, as demonstrated in both the Supplementary Materials and Fig. S1.

Identify the determinants of VPD response

We assessed the determinants of growth response to VPD through the relationship between the significant *t*-values of growth-VPD relationship and seven environmental, tree species and forest structure variables, namely site elevation, mean annual temperature (MAT), mean annual precipitation (MAP), summer SMI, tree species, mean tree age and BA at site level.

Tree species and forest structure variables

Among the significant variables, species identity displayed the lowest average depth in the random forest decision trees and was selected as root node in 158 of 500 trees, meaning it is the first variable determining the direction and strength of growth-VPD *t*-values (Fig. 3, Table 1). The species showing more negative VPD growth responses were *Picea glauca, Pinus resinosa, Pseudotsuga menziesii*, and *Pinus contorta* while *Abies lasiocarpa, Picea engelmanii*, *Populus tremuloides* and *Pinus contorta* showed a less negative response to VPD. Site-level mean tree age displayed the second lowest average depth and was selected as a root node in 68 of 500 decision trees (Fig. 3, Table 1). Mean tree age was generally positively correlated with *t*-values (Fig. 4), meaning a more negative response to VPD occurred in young to mature trees (0-100 years) compared to mature and old trees (100–250 years); a low sample size hinders the capacity to infer the typical growth response to VPD beyond 250 years of mean tree age. Site-level mean BA displayed high average depth and very low MSE, meaning it makes a minor contribution to *t*-value variations.

Local environmental and climatic variables

Among significant variables, long-term mean summer SMI was the primary determinant of *t*-values, with the lowest average depth among random forest trees and higher selection as root node (for 158 of 500 trees). Mean summer SMI was positively correlated with *t*-values, meaning the most detrimental effects of VPD were seen in sites with low available soil water (Fig. 4). Local MAT displayed the second lowest average depth and was selected as root node in 117 decision trees (Fig. 3, Table 1). MAT was negatively correlated with *t*-values, meaning VPD had a more negative effect on growth in higher MAT environments or during warmer years (Fig. 4).

Spatiotemporal changes in VPD and growth of widespread tree species

Central and northern Canadian boreal regions have experienced significant increases in summer VPD since 1951 (Fig. 5a). The affected regions extend across the ranges of *Picea mariana* and *Picea glauca* (Fig. 1). At these locations, mean VPD values increased from slightly above 0.5 kPa in the 1950s-1960s to > 0.6 kPa in the 2000s. We found that percent growth changes (GC) in terms of BAI, averaged by species, were linearly and inversely related to prior-summer VPD (Fig. 5b-c). From the slope of this relationship, we estimated that for every ~ 0.1 kPa increase in VPD, there was a ~10 to 11% decrease in mean BAI throughout the geographic ranges of these spruce species (Fig. 5b-c). Decreases in tree growth from 1951 to present were apparent in both species, paralleling the increases of summer VPD. Although the northern part of region was sparsely sampled among our ~ 4,000 sites, as the diameter growth of both species is negatively affected by high prior-summer VPD values (Fig. 2, 5), we might expect a negative growth response for these species in this region in the decades ahead. We also examined the same relationship for two other species that showed significant growth sensitivity to VPD, *Pinus contorta* and *Picea engelmannii* (Fig. 5d-e). Again, the percent change in growth averaged across *Pinus contorta* was linearly correlated with prior-summer VPD, but to a much lesser extent than in the two spruces. For *Picea engelmannii*, there was no evidence for a negative relation of range-wide averaged growth change to prior-summer VPD ($r = -0.18$ with 95% CI [-0.44; 0.12]), but rather a moderate positive relationship to current-summer VPD (Fig. 5d).

Discussion

We show that increasing atmospheric drought has negatively impacted growth in all nine major boreal forest species assessed. The main response to increasing VPD was a first growth reduction for the current growing season in some species, before a second, larger, growth reduction the following year that was widespread across species. These findings corroborate those observed in several temperate forests, specifically the lag between carbon uptake, measured from flux towers, and carbon allocation to wood the following year, assessed by tree-ring measurements. This lag, while not well understood, is often assumed to be controlled by allocation to non-structural carbon (NSC) storage, which is induced by current conditions and increases resistance and/or resilience to future drought (Cabon et al., 2022; Teets et al., 2022).

To optimize the balance between carbon gain and water loss, trees attempt to balance between water uptake and losses regulated by leaf water potential and associated stomatal conductance (Ewers et al., 2005; Hochberg et al., 2018). Increases in VPD and subsequent drought risk typically induce a decrease in stomatal aperture and conductance to regulate leaf-level transpiration. Stomatal sensitivity to VPD is typically higher in *Abies lasiocarpa*, *Pinus contorta*, *Populus tremuloides*, and *Pseudotsuga menziesii*, which maintain more constant leaf water potential via stomatal closure (more isohydric), and lower in *Picea mariana* and *Picea engelmannii* which allow a greater drop in leaf water potential (more anisohydric species; Grossior et al., 2020; Pappas et al., 2018; Arango-Velez et al., 2016; Zhang et al., 2020; Kerhoulas et al., 2020; Bansal et al., 2015). That being said, a clear pattern in tree growth response to VPD matching this iso/anisohydric continuum was not observed, with isohydric species being either among the most sensitive (*Pseudotsuga menziesii* or *Pinus contorta*) or the less sensitive to VPD (*Populus tremuloides* and *Abies lasiocarpa*). The absence of a clear pattern could be due to species growing in different environments across this broad spatial area, making it difficult to isolate a species effect or to observe differences in their water-use strategies.

Variation in the strength of tree responses to VPD was not just determined by species, but also by MAT (an effect that persisted after removing the indirect effect of soil moisture) and by local summer SMI. This growth sensitivity to VPD confirmed that warming and drying impact boreal forest growth by increasing tree sensitivity to atmospheric water demand (Reich et al., 2018; López et al., 2021). Heightened growth sensitivity to VPD at higher temperatures and lower soil moisture is also consistent with a potential physiological mechanism; as data for more than a dozen species show acclimation to warmer temperatures and lower soil moisture via shifts to a more conservative stomatal behavior that saves more water at the cost of gaining less carbon (Stefanski et al., 2022).

In contrast, some sites, largely contiguous with eastern Boreal and Taiga Shields and in the Boreal Cordillera, showed a positive growth response to increasing VPD. This positive response to VPD is likely limited to sites where growth is enhanced by a temperature increase while VPD remains low without becoming stressful, typically sites with low mean annual temperatures, excess soil moisture, and/or short growing seasons (López et al., 2021; Pau et al., 2022; Oogathoo et al., 2022). In particular, excess water in the soil and shallow water table can contribute to hypoxia or anoxia (*i.e.* oxygen deficiency or absence) in belowground plant tissues, a phenomenon that ultimately leads to a decrease in root hydraulic conductance and reduces tree growth (Liu et al., 2022). Atmospherically enhanced evapotranspiration with warming could mitigate these negative effects and lead to a positive effect of rising VPD on tree growth. Additionally, in colder parts of the species' ranges, the warmer temperatures associated with higher VPD could alleviate cold limitations of growth more than a quite modest increase in VPD would limit stomatal conductance.

The strength of tree responses to VPD depended on average tree age in the sampled site. The growth response to rising VPD was most negative for young trees, and the strength of the response decreased steadily with average site age until reaching a plateau around an average tree age of 200 years. There have been reports that wood with juvenile anatomical traits may be more vulnerable to cavitation than mature wood owing to thinner tracheid walls (Zobel et al., 2012; Lu et al., 2021). The need for NSC storage after a drought event would hence be higher at this early stage,

consistent with lower overall biomass and a not-yet fully developed root system (Ewers et al., 2005). Stomatal response to VPD is known to change with tree age, along with tree growth sensitivity to drought, which makes trees more sensitive to water stress over time (Voelker et al., 2011; Zhang et al., 2020).

The extent of the area showing sensitivity to atmospheric drought is much larger than some modeling studies and satellite imagery analysis had suggested (e.g. Aubin et al., 2018; Mirabel et al., 2022; Sang et al., 2022). Such a broad extent likely reflects the multiple mechanisms linking growth to atmospheric dryness, directly through stomatal conductance reducing growth or indirectly through soil moisture levels (Novick et al., 2016; Massmann et al., 2019; Grossiord et al., 2020; Liu et al., 2020; López et al., 2021; Lu et al., 2022). Regarding indirect effects through soil moisture levels, however, additional assessments of our data suggested that VPD effects were not confounded by co-variation in soil moisture in the majority of studied sites. For all species, the amount of significant VPD effects on growth remained after removing the partial effect of soil moisture on growth increment (see Supplementary Materials and Fig. S1). These findings are consistent with recent reports suggesting that stomatal sensitivity to VPD represents the primary response to rising VPD (Grossiord et al., 2020; Lu et al., 2022).

Climate change is expected to lead to an overall increase in temperatures across Canada (https://atlasclimatique.ca/) and although an increase in spring or early summer rainfall is expected, this would not compensate for the warming-induced increase in VPD for some regions (Vincent et al., 2018). However, the specific impacts of climate change on VPD depend on a variety of factors, including changes in humidity, evaporation, and precipitation patterns (Yuan et al., 2019). Our results indicate that tree growth across Canada is strongly related to VPD and that growth in widespread species like *Picea mariana*, *Picea glauca* and *Pinus banksiana* is already being suppressed by increasing atmospheric drought. We can anticipate that further warming and precipitation changes over the next century will continue to hamper the growth of these common boreal species (Zhang et al., 2020). Such understanding should foster insights for developing adaptive measures aiming at improving forest resistance to drought conditions (Kerhoulas et al., 2020; Achim et al., 2022).

Methods

Study area

The study area covers eleven forested ecozones (Ecological Stratification Working Group (ESWG), 1996) in Canada (Fig. 1). These ecozones are the Pacific Maritime in the west coast, the Montane Cordillera, Boreal Cordillera and Taiga Cordillera that contain the Canadian Rockies, the Boreal Plains and Taiga Plains located east of the Rockies, and Taiga Shield, Boreal Shield and Hudson Plains in the continental interior to the east. Bounded by three Great Lakes in the east are the Mixedwood Plains, and adjacent to the east coast is the Atlantic Maritime (Fig. 1). The climate in the boreal/hemi-boreal zone is predominantly high-latitude continental, with long cold winters, short cool summers, and relatively low annual precipitation, but with significant regional variation (Price et al., 2013). Summer mean air temperature averages from 10°C in the Taiga Cordillera to 14°C in the Atlantic Maritime, whereas winter mean air temperature ranges from − 22.0°C in the Taiga Cordillera to − 1.5°C in the Pacific Maritime. Annual precipitation totals average from 200–500 mm in the Taiga Plains to over 4,000 mm in the Pacific Maritime.

Climatic data

Daily maximum, minimum and dew point temperature (ºC), precipitation (mm), and relative humidity (%) were obtained for the period from 1950 to 2018 using BioSIM v10.3 software, which interpolates site-specific estimates from all of Environment Canada's (2013) historical weather observations (Régnière & Bolstad, 1994; Régnière et al., 2014). Based

on the daily minimum, maximum and dew point temperature observations, BioSIM returned daily vapour pressure deficit (VPD, in kPa), the difference between actual atmospheric water vapour amount and the maximum amount at saturation for a given temperature (Allen et al., 1998). BioSIM also calculates a soil moisture index (SMI, in % of water holding capacity), using a quadratic-plus-linear formulation procedure (Hogg et al., 2013) based on water lost by evapotranspiration and gained from precipitation. A low SMI is an indication of low available soil water at the site. Daily temperature, precipitation, VPD, and SMI data were all interpolated to a 1° x 1° grid (n = 604 grid cells). VPD and SMI data were averaged for the summer season (June to August) by year, and attributed to the closest tree-ring sampling sites of grid cells' centroid. In addition, long-term means of annual climatologies (1951–2018) were also computed for each site (mean annual January to December temperature, MAT, mean annual January to December sums of precipitation, MAP, and mean summer soil moisture index, SMI).

Tree-ring data

Annual tree-ring width data were retrieved from the Canadian Forest Service Tree-Ring repository (CFS-TRenD 1.0; Girardin et al., 2021b), developed with the goal of combining data from different sources and making them available in a consistent format for large-scale analyses. CFS-TRenD contains measurements from 40,206 samples from 4,594 sites and 62 tree species. The primary national-scale dataset in CFS-TRenD 1.0 is increment cores sampled since 2001 during the establishment of Canada's National Forest Inventory (NFI, Gillis et al., 2005). The NFI network, designed to represent species distributions and their range of growing conditions in Canada, comprises 6,010 core samples from 870 sites. Other important data are more regional and include data from a network of permanent sample plots established by the Alberta Biodiversity Monitoring Institute (ABMI), a network of temporary sample plots established by the Ministère des Ressources Naturelles et de la Faune du Québec (MFFPQ; Programme d'inventaire écoforestier nordique, Létourneau et al., 2008; Girardin et al., 2021b), and the Climate Impacts on Productivity and Health of Aspen (CIPHA) network (Hogg et al., 2005). Additional contributions to CFS-TRenD are from smaller-scale projects carried out by individual researchers, and data extracted from the International Tree-Ring Data Bank (ITRDB).

Analyses were limited to the nine dominant species (seven genera) in the dataset (Fig. 1) to maintain a sampling density that balances local variations in growth across sampling sites within regions, and detects growth sensitivity to climate at the regional scale. These nine species represent 80% of the samples (32,189 trees) in the CFS-TRenD repository: *Picea mariana* (black spruce; 25% of the dataset with 1.0 e^4 trees sampled), *Picea glauca* (white spruce; 12%, 4.7 e^3 trees), *Pinus banksiana* (jack pine; 11%, 4.4 e^3 trees), *Populus tremuloides* (trembling aspen; 10%, 3.9 e^3 trees), *Pinus contorta* (lodgepole pine; 7%, 2.9 e^3 trees), *Pseudotsuga menziesii* (Douglas fir; 7%, 2.8 e^3 trees), *Picea engelmannii* (Engelmann spruce; 4%, 1.7 e^3 trees), *Abies lasiocarpa* (subalpine fir; 2%, 9.3 e^2 trees), and *Pinus resinosa* (red pine; 2%, 8.7 e^2 trees). We excluded *Abies balsamea* (balsam fir, mostly dominant in the eastern ecozones) because its growth dynamics are strongly influenced by spruce budworm (*Choristoneura fumiferana*) defoliation (Lavoie et al., 2019; Sánchez-Pinillos et al., 2019). All of the nine species occur in Canadian boreal/hemi-boreal forests (Brandt et al., 2013). Half of the sites included two or three sampled trees, and 83% of the sites included a single species. Fifty percent of the trees displayed between 40 and 90 measured tree rings (i.e. 25th and 75th percentiles of the age distribution). Both visual and statistical quality control procedures were applied to ensure that only true growth rings were measured and that the correct calendar year was assigned to each tree-ring (Girardin et al., 2021b). In an analysis of sample coherency, Girardin et al. (2021b) found high spatial synchronicity in the interannual growth fluctuations among most samples.

Responsiveness of tree growth to vapour pressure deficit

Calculation of basal area increments.

Tree-level average ring-width series were converted to annual basal area increments (BAI; $cm^2\ yr^{-1}$), which is recognized to be closely related to tree productivity (Babst et al., 2014). BAI was estimated from the relation:

eq 1. $$BAI_t = \pi R_t^2 - \pi R_{t-1}^2$$

Where R_t and R_{t-1} are the stem radii (cm) at the end and beginning of a given annual ring increment. Minimum tree age was determined from ring counts, starting from the outermost ring. As strong differences in growth occur between trees' early and mature development stages, we excluded tree-rings formed during the first ten years from later analyses (Loader et al., 2007).

Growth And Climate Relationships

Species-specific growth-VPD relationships were determined using generalized additive mixed models (GAMM) fitted at each site between the log-transformed BAI series, tree basal area of the year prior to ring formation and atmospheric VPD values during summer (June, July and August) of the prior and current year of ring formation, with tree considered as a random effect:

eq 2.
$$log\left(BAI_{jk}^{t}\right) = \beta_{jk}.log\left(BA_{jk}^{t-1}\right) + s\left(age^{t}\right) + \mathrm{VPD}^{t-1} + \mathrm{VPD}^{t} + corAR1_{jk}\left(\tilde{t}\,\middle|\,Tree_{ID}\right) + Tree_{ID} + \epsilon_{jkt}$$

Where *i* stands for tree identity, *j* for the species, *k* for the site, and *t* for the year. *BA* is the basal area, *BAI* is the basal area increment, *age* is the age in years, and *s* is a cubic regression spline smoothing parameter whose degree of smoothness was determined through an iterative fitting process. Temporal autocorrelation was considered with *AR1*, an autoregressive term of order 1 accounting for year *t* and $Tree_{ID}$ (each tree's unique identifier). The significance of variables at the 5% level was determined from *t*-test*s* in GAMM models (*t*-value's $p < 0.05$). The growth model was fitted using the mgcv R package (Wood, 2006).

Drivers Of Growth Sensitivity To Vpd

Environmental, tree species and forest structure variables responsible for the observed distribution in VPD-growth relationships (*i.e. t*-values) were assessed as follows. These analyses were guided by the hypothesis that the strongest negative responses to VPD would be observed at sites exposed to high temperatures or with low soil water availability. We also postulated that there is differentiation among species' responses to VPD resulting from their evolutionary strategy for stomatal conductance. We considered four environmental variables (elevation, mean annual temperature (MAT), mean annual precipitation (MAP), and summer SMI), tree species, and two forest structure variables (mean site age and basal area (BA)). First, we used the Random Forests (RF) algorithm, a machine learning method adapted to complex and potentially non-linear relationships (Breiman, 2001). Our RF was based on the bootstrap of 500 training decision trees aggregated to predict the *t*-values of the significant ($p < 0.05$) growth-VPD_t or growth-VPD_{t-1} relationships, using the seven predictor variables as the potential explanatory variables. The running and interpretation of the RF were performed using 'randomForest' and 'randomForestExplainer' R packages (Liaw et al., 2002; Paluszynska et al., 2020). Variable importance was measured as the decrease of unscaled mean square error (MSE decrease) observed when the variable is randomized, and averaged among training trees (Strobl et al., 2008). We retrieved variables' average depth among training trees and their occurrence as the first node. Finally, to get the direction of the relationship between variables and *t*-values, we drew the partial dependence plot representing the

marginal effect of each variable on the *t*-values. To untangle the direct VPD effect of atmospheric dryness on stomatal conductance from its indirect effect on soil moisture, we examined partial BAI-VPD GAMM models obtained after controlling for the effect of soil moisture index (SMI) on growth (see Supplementary Materials and Fig. S1).

Trends In Vpd And Growth

Annual fluctuations in growth over time were obtained from the detrending of BAI series that removed growth trends due to tree age and size (Zhang et al., 2018). We detrended time series of BAI using GAMMs fitted to the log-transformed BAI:

$$\text{eq 3.} \log\left(BAI_{ijk}^{t}\right) = \beta_{jk}.\log\left(BAI_{ijk}^{t-1}\right) + s_i\left(cambial\ age_{ijk}^{t}\right) + Z_{jk}B_{jk} + \nu_{jk} + \epsilon_{jk}^{t}$$

Annual growth changes (GC), expressed as the percent deviation from predicted values generated by the GAMMs, were then computed following (Girardin et al., 2016b). GC was average by species and year to show yearly temporal variability in species-specific GC since 1951. The average GC 95% confidence interval was computed at the species level, for each calendar year, by correcting the effective degrees of freedom (*n*') based on first-order (*i.e.*, lag = 1) autocorrelation estimates of Moran's I (Dale and Fortin, 2002) (moran.test function in R). Correlations (*r*) between growth changes and VPD were computed from a bootstrapping technique that accounted for autocorrelation and trends in data (Mudelsee and Alkio, 2007), and regression slope (β_1) from ordinary-least-square regressions.

Linear trends of summer VPD were examined for 1951–2018 using least squares linear regressions. A derivation of *t* test with an estimate of the effective sample size accounting for serial persistence in data returned the slope's significance against the null hypothesis that the trend is different from zero (Storch and Zwiers, 1999).

Declarations

Author contributions

M.P.G, D.W., and A.M. conceived this work, A.M. and M.P.G. wrote the original manuscript. All authors discussed and interpreted the results and contributed to the manuscript.

Data Availability

Weather data that support the finding of this study are freely accessible through Environment and Climate Change Canada's portal (https://climate.weather.gc.ca/) and the BioSIM server (https://cfs.nrcan.gc.ca/projects/133). Tree-ring datasets were deposited in the Natural Resources Canada TreeSource repository https://treesource.rncan.gc.ca/en. Restrictions may apply to the availability of third-party data (contact details are included in the TreeSource repository). The data that support the plots within this paper and other findings of this study are available from the corresponding authors upon reasonable request.

Code Availability

All relevant software and R-functions that support the methods of this study are referred to in the "Methods" section (see package vignettes for details).

References

1. Achim, A., Moreau, G., Coops, N. C., Axelson, J. N., Barrette, J., Bédard, S., … White, J. C. (2022). The changing culture of silviculture. Forestry, 95(2), 143–152.
2. Allen, R. G., Pereira, L. S., Raes, D., & Smith, M. (1998). Crop evapotranspiration - Guidelines for computing crop water requirements - FAO Irrigation and drainage paper 56. Fao, Rome, 300(9), D05109.
3. Arango-Velez, A., El Kayal, W., Copeland, C. C., Zaharia, L. I., Lusebrink, I., & Cooke, J. E. (2016). Differences in defence responses of *Pinus contorta* and *Pinus banksiana* to the mountain pine beetle fungal associate Grosmannia clavigera are affected by water deficit. Plant, Cell & Environment, 39(4), 726–744.
4. Aubin, I., Boisvert-Marsh, L., Kebli, H., McKenney, D., Pedlar, J., Lawrence, K., Hogg, E. H., Boulanger, Y., Gauthier, S., & Ste-Marie, C. (2018). Tree vulnerability to climate change: Improving exposure-based assessments using traits as indicators of sensitivity. Ecosphere, 9(2), e02108.
5. Babst, F., Bouriaud, O., Papale, D., Gielen, B., Janssens, I. A., Nikinmaa, E., Ibrom, A., Wu, J., Bernhofer, C., Köstner, B., & others. (2014). Above-ground woody carbon sequestration measured from tree rings is coherent with net ecosystem productivity at five eddy-covariance sites. *New Phytologist*, 201(4), 1289–1303.
6. Babst, F., Bouriaud, O., Poulter, B., Trouet, V., Girardin, M. P., & Frank, D. C. (2019). Twentieth century redistribution in climatic drivers of global tree growth. Science Advances, 5(1), eaat4313.
7. Bansal, S., Harrington, C. A., Gould, P. J., & St. Clair, J. B. (2015). Climate-related genetic variation in drought-resistance of Douglas-fir (*Pseudotsuga menziesii*). Global Change Biology, 21(2), 947–958.
8. Boucher, D., Boulanger, Y., Aubin, I., Bernier, P. Y., Beaudoin, A., Guindon, L., & Gauthier, S. (2018). Current and projected cumulative impacts of fire, drought, and insects on timber volumes across Canada. Ecological Applications, 28(5), 1245–1259.
9. Brandt, J. P., Flannigan, M. D., Maynard, D. G., Thompson, I. D., & Volney, W. J. A. (2013). An introduction to Canada's boreal zone: ecosystem processes, health, sustainability, and environmental issues. Environmental Reviews, 21(4), 207–226.
10. Breiman, L. (2001). Random forests. Machine Learning, 45(1), 5–32.
11. Ecological Stratification Working Group (ESWG) (1996) A national ecological framework for Canada. Agriculture and Agri-Food Canada and Environment Canada, Ottawa
12. Cabon, A., Kannenberg, S. A., Arain, A., Babst, F., Baldocchi, D., Belmecheri, S., Delpierre, N., Guerrieri, R., Maxwell, J. T., McKenzie, S., & others. (2022). Cross-biome synthesis of source versus sink limits to tree growth. *Science*, 376(6594), 758–761
13. de Cárcer, P., Vitasse, Y., Peñuelas, J., Jassey, V. E. J., Buttler, A., & Signarbieux, C. (2018). Vapor–pressure deficit and extreme climatic variables limit tree growth. Global Change Biology, 24(3), 1108–1122.
14. Critchfield, W. B., & Little, E. L. (1966). Geographic distribution of the pines of the world (Issue 991). US Department of Agriculture, Forest Service.
15. Dale, M. R. T., & Fortin, M.-J. (2002). Spatial autocorrelation and statistical tests in ecology. Ecoscience, 9(2), 162–167.
16. Danneyrolles, V., Boucher, Y., Fournier, R., & Valeria, O. (2022). Positive effects of projected climate change on post-disturbance forest regrowth rates in northeastern North American boreal forests. *Environmental Research Letters*.
17. Denissen, J., Teuling, A. J., Pitman, A. J., Koirala, S., Migliavacca, M., Li, W., Reichstein, M., Winkler, A. J., Zhan, C., & Orth, R. (2022). Widespread shift from ecosystem energy to water limitation with climate change. Nature Climate Change, 12(7), 677–684.

18. Evans, M. E., DeRose, R. J., Klesse, S., Girardin, M. P., Heilman, K. A., Alexander, M. R., … GaytÁn, S. A. V. (2022). Adding tree rings to North America's national forest inventories: An essential tool to guide drawdown of atmospheric CO2. *BioScience*, 72(3), 233–246.
19. Ewers, B. E., Gower, S. T., Bond-Lamberty, B., & Wang, C. K. (2005). Effects of stand age and tree species on canopy transpiration and average stomatal conductance of boreal forests. Plant, Cell & Environment, 28(5), 660–678.
20. Gillis, M. D., Omule, A. Y., & Brierley, T. (2005). Monitoring Canada's forests: the national forest inventory. The Forestry Chronicle, 81(2), 214–221.
21. Girardin, M. P., Hogg, E. H., Bernier, P. Y., Kurz, W. A., Guo, X. J., & Cyr, G. (2016a). Negative impacts of high temperatures on growth of black spruce forests intensify with the anticipated climate warming. Global Change Biology, 22(2), 627–643.
22. Girardin, M. P., Bouriaud, O., Hogg, E. H., Kurz, W., Zimmermann, N. E., Metsaranta, J. M., de Jong, R., Frank, D. C., Esper, J., Büntgen, U., & others. (2016b). No growth stimulation of Canada's boreal forest under half-century of combined warming and CO2 fertilization. *Proceedings of the National Academy of Sciences*, 113(52), E8406–E8414.
23. Girardin, M. P., Isabel, N., Guo, X. J., Lamothe, M., Duchesne, I., & Lenz, P. (2021a). Annual aboveground carbon uptake enhancements from assisted gene flow in boreal black spruce forests are not long-lasting. Nature Communications, 12(1), 1–15.
24. Girardin, M. P., Guo, X. J., Metsaranta, J., Gervais, D., Campbell, E., Arsenault, A., Isaac-Renton, M., Harvey, J. E., Bhatti, J., & Hogg, E. H. (2021b). A national tree-ring data repository for Canadian forests (CFS-TRenD): structure, synthesis, and applications. Environmental Reviews, 29(2), 225–241.
25. Grossiord, C., Buckley, T. N., Cernusak, L. A., Novick, K. A., Poulter, B., Siegwolf, R. T. W., Sperry, J. S., & McDowell, N. G. (2020). Plant responses to rising vapor pressure deficit. New Phytologist, 226(6), 1550–1566.
26. Hammond, W. M., Williams, A. P., Abatzoglou, J. T., Adams, H. D., Klein, T., López, R., Sáenz-Romero, C., Hartmann, H., Breshears, D. D., & Allen, C. D. (2022). Global field observations of tree die-off reveal hotter-drought fingerprint for Earth's forests. Nature Communications, 13(1), 1–11.
27. Hochberg, U., Rockwell, F. E., Holbrook, N. M., & Cochard, H. (2018). Iso/anisohydry: a plant–environment interaction rather than a simple hydraulic trait. Trends in plant science, 23(2), 112–120.
28. Hogg, E. H., Brandt, J. P., & Kochtubajda, B. (2005). Factors affecting interannual variation in growth of western Canadian aspen forests during 1951–2000. Canadian Journal of Forest Research, 35(3), 610–622.
29. Hogg, E. H., Barr, A. G., & Black, T. A. (2013). A simple soil moisture index for representing multi-year drought impacts on aspen productivity in the western Canadian interior. Agricultural and Forest Meteorology, 178, 173–182.
30. IPCC, Masson-Delmotte, V., Zhai, P., Pirani, A., Connors, S. L., Péan, C., Berger, S., … Zhou, B. (2021). Climate change 2021: the physical science basis. Contribution of working group I to the sixth assessment report of the intergovernmental panel on climate change, 2.
31. Kerhoulas, L., Polda, W., Kerhoulas, N., & Berrill, J. P. (2020). Physiology and growth of Douglas-fir and redwood seedlings planted after partial harvesting. Frontiers in Forests and Global Change, 49.
32. Lavoie, J., Montoro Girona, M., & Morin, H. (2019). Vulnerability of conifer regeneration to spruce budworm outbreaks in the eastern Canadian boreal forest. Forests, 10(10), 850.
33. Létourneau, J. P., Matejek, S., Morneau, C., Robitaille, A., Roméo, T., Brunelle, J., & Leboeuf, A. (2008). Norme de cartographie écoforestière du Programme d'inventaire écoforestier nordique. Ministère Des Ressources Naturelles et de La Faune Du Québec: Québec, QC.

34. Liaw, A., Wiener, M., & others. (2002). Classification and regression by randomForest. *R News*, 2(3), 18–22.
35. Little, E. L., & Viereck, L. A. (1971). Atlas of United States Trees:(no. 1146). Conifers and important hardwoods, by EL Little, Jr (Vol. 1, Issue 1146). US Government printing office.
36. Liu, L., Gudmundsson, L., Hauser, M., Qin, D., Li, S., & Seneviratne, S. I. (2020). Soil moisture dominates dryness stress on ecosystem production globally. Nature Communications, 11(1), 1–9.
37. Liu, C., Wang, Q., Mäkelä, A., Hökkä, H., Peltoniemi, M., & Hölttä, T. (2022). A model bridging waterlogging, stomatal behavior and water use in trees in drained peatland. Tree Physiology, 42(9), 1736–1749.
38. Loader, N. J., McCarroll, D., Gagen, M., Robertson, I., & Jalkanen, R. (2007). Extracting climatic information from stable isotopes in tree rings. Terrestrial Ecology, 1, 25–48.
39. López, J., Way, D. A., & Sadok, W. (2021). Systemic effects of rising atmospheric vapor pressure deficit on plant physiology and productivity. Global Change Biology, 27(9), 1704–1720.
40. Lu, H., Qin, Z., Lin, S., Chen, X., Chen, B., He, B., Wei, J., & Yuan, W. (2022). Large influence of atmospheric vapor pressure deficit on ecosystem production efficiency. Nature Communications, 13(1), 1–4.
41. Lu, C., Wu, J., Jiang, Q., Liu, Y., Zhou, L., You, Y., … Liu, S. (2021). Influence of juvenile and mature wood on anatomical and chemical properties of early and late wood from Chinese fir plantation. Journal of Wood Science, 67(1), 1–11.
42. Massmann, A., Gentine, P., & Lin, C. (2019). When does vapor pressure deficit drive or reduce evapotranspiration? Journal of Advances in Modeling Earth Systems, 11(10), 3305–3320.
43. Mirabel, A., Girardin, M. P., Metsaranta, J., Campbell, E. M., Arsenault, A., Reich, P. B., & Way, D. (2022). New tree-ring data from Canadian boreal and hemi-boreal forests provide insight for improving the climate sensitivity of terrestrial biosphere models. Science of the Total Environment, 851, 158062.
44. Mudelsee, M., & Alkio, M. (2007). Quantifying effects in two-sample environmental experiments using bootstrap confidence intervals. Environmental Modelling & Software, 22(1), 84–96.
45. Novick, K. A., Ficklin, D. L., Stoy, P. C., Williams, C. A., Bohrer, G., Oishi, A. C., Papuga, S. A., Blanken, P. D., Noormets, A., Sulman, B. N., & others. (2016). The increasing importance of atmospheric demand for ecosystem water and carbon fluxes. *Nature Climate Change*, 6(11), 1023–1027.
46. Oogathoo, S., Houle, D., Duchesne, L., & Kneeshaw, D. (2022). Evaluation of simulated soil moisture and temperature for a Canadian boreal forest. Agricultural and Forest Meteorology, *323*, 109078.
47. Paluszynska, A., Biecek, P., & Jiang, Y. (2020). randomForestExplainer: Explaining and Visualizing Random Forests in Terms of Variable Importance.
48. Pappas, C., Matheny, A. M., Baltzer, J. L., Barr, A. G., Black, T. A., Bohrer, G., … Stephens, J. (2018). Boreal tree hydrodynamics: asynchronous, diverging, yet complementary. Tree physiology, 38(7), 953–964.
49. Pau, M., Gauthier, S., Chavardès, R. D., Girardin, M. P., Marchand, W., & Bergeron, Y. (2022). Site index as a predictor of the effect of climate warming on boreal tree growth. Global Change Biology, 28(5), 1903–1918.
50. Peng, C., Ma, Z., Lei, X., Zhu, Q., Chen, H., Wang, W., Liu, S., Li, W., Fang, X., & Zhou, X. (2011). A drought-induced pervasive increase in tree mortality across Canada's boreal forests. Nature Climate Change, 1(9), 467–471.
51. Price, D. T., Alfaro, R. I., Brown, K. J., Flannigan, M. D., Fleming, R. A., Hogg, E. H., Girardin, M. P., Lakusta, T., Johnston, M., McKenney, D. W., & others. (2013). Anticipating the consequences of climate change for Canada's boreal forest ecosystems. *Environmental Reviews*, 21(4), 322–365.
52. Régnière, J., & Bolstad, P. (1994). Statistical simulation of daily air temperature patterns in eastern North America to forecast seasonal events in insect pest management. Environmental Entomology, 23(6), 1368–1380.

53. Régnière, J., Saint-Amant, R., Béchard, A., & Moutaoufik, A. (2014). BioSIM 10: User's manual. Laurentian Forestry Centre.
54. Reich, P. B., Sendall, K. M., Stefanski, A., Rich, R. L., Hobbie, S. E., & Montgomery, R. A. (2018). Effects of climate warming on photosynthesis in boreal tree species depend on soil moisture. Nature, 562(7726), 263–267.
55. Reich, P. B., Bermudez, R., Montgomery, R. A., Rich, R. L., Rice, K. E., Hobbie, S. E., & Stefanski, A. (2022). Even modest climate change may lead to major transitions in boreal forests. Nature, 608(7923), 540–545.
56. Sánchez-Pinillos, M., Leduc, A., Ameztegui, A., Kneeshaw, D., Lloret, F., & Coll, L. (2019). Resistance, resilience or change: post-disturbance dynamics of boreal forests after insect outbreaks. Ecosystems, 22(8), 1886–1901.
57. Sang, Z., & Hamann, A. (2022). Climatic limiting factors of North American ecosystems: a remote-sensing based vulnerability analysis. Environmental Research Letters, 17(9), 094011.
58. Serreze, M. C., Walsh, J. E., Chapin, F. S., Osterkamp, T., Dyurgerov, M., Romanovsky, V., Oechel, W. C., Morison, J., Zhang, T., & Barry, R. G. (2000). Observational evidence of recent change in the northern high-latitude environment. Climatic Change, 46(1), 159–207.
59. Spawn, S. A., & Gibbs, H. K. (2020). Global aboveground and belowground biomass carbon density maps for the year 2010. Ornl Daac.
60. Stefanski, A., Butler, E. E., Bermudez, R., Montgomery, R. A., & Reich, P. B. (2022). Stomatal behavior moderates water cost of CO2 acquisition for 21 boreal and temperate species under experimental climate change. Plant, Cell & Environment.
61. Von Storch, H., & Zwiers, F. W. (2002). *Statistical analysis in climate research*. Cambridge university press.
62. Strobl, C., Boulesteix, A.-L., Kneib, T., Augustin, T., & Zeileis, A. (2008). Conditional variable importance for random forests. BMC Bioinformatics, 9(1), 1–11.
63. Teets, A., Moore, D. J. P., Alexander, M. R., Blanken, P. D., Bohrer, G., Burns, S. P., Carbone, M. S., Ducey, M. J., Fraver, S., Gough, C. M., & others. (2022). Coupling of Tree Growth and Photosynthetic Carbon Uptake Across Six North American Forests. *Journal of Geophysical Research: Biogeosciences*, 127(4), e2021JG006690.
64. Vincent, L. A., Zhang, X., Mekis, É., Wan, H., & Bush, E. J. (2018). Changes in Canada's climate: Trends in indices based on daily temperature and precipitation data. Atmosphere-Ocean, 56(5), 332–349.
65. Voelker, S. L. (2011). Age-dependent changes in environmental influences on tree growth and their implications for forest responses to climate change. Size-and age-related changes in tree structure and function, 455–479.
66. Wulder, M. A., Hermosilla, T., White, J. C., & Coops, N. C. (2020). Biomass status and dynamics over Canada's forests: Disentangling disturbed area from associated aboveground biomass consequences. Environmental Research Letters, 15(9), 094093.
67. Wood, S. N. (2006). Generalized additive models: an introduction with R.
68. Yuan, W., Zheng, Y., Piao, S., Ciais, P., Lombardozzi, D., Wang, Y., Ryu, Y., Chen, G., Dong, W., Hu, Z., & others. (2019). Increased atmospheric vapor pressure deficit reduces global vegetation growth. *Science Advances*, 5(8), eaax1396.
69. Zhang, Z., Babst, F., Bellassen, V., Frank, D., Launois, T., Tan, K., Ciais, P., & Poulter, B. (2018). Converging climate sensitivities of European forests between observed radial tree growth and vegetation models. Ecosystems, 21(3), 410–425.
70. Zhang, Q., Ficklin, D. L., Manzoni, S., Wang, L., Way, D., Phillips, R. P., & Novick, K. A. (2019). Response of ecosystem intrinsic water use efficiency and gross primary productivity to rising vapor pressure deficit. Environmental Research Letters, 14(7), 074023.
71. Zhang, L., Liu, L., Zhao, H., Jiang, Z., & Cai, J. (2020). Differences in near isohydric and anisohydric behavior of contrasting poplar hybrids (i-101 (populus alba l.)× 84k (*populus alba* l.× *populus glandulosa* uyeki)) under

drought-rehydration treatments. Forests, 11(4), 402.

72. Zhang, L., Wang, R., Liu, X., Ran, Y., Shang, S., & Liu, X. (2020). Age-and region-related response of radial growth to climate warming and a warming hiatus. Trees, *34*, 199–212.
73. Zobel, B. J., & Sprague, J. R. (2012). *Juvenile wood in forest trees*. Springer Science & Business Media.

Table

Table 1

Output of the random forest algorithm: average depth of variables in trees, average increase in dataset mean squared error (MSE) after variable permutation, and variable occurrences as tree root node. Results based on bootstrap with 500 decision trees. MAP: mean annual precipitation, MAT: mean annual temperature, BA: basal area, SMI: soil moisture index.

Variable	Average minimum depth	Average MSE increase	Occurrences as root node
Elevation	2.43	1.33	25
MAP	2.27	3.16	31
MAT	1.55	2.42	117
Summer SMI	1.74	2.91	96
Species	1.16	2.31	158
Mean age	1.53	1.12	68
Mean BA	3.31	-0.18	5

Figures

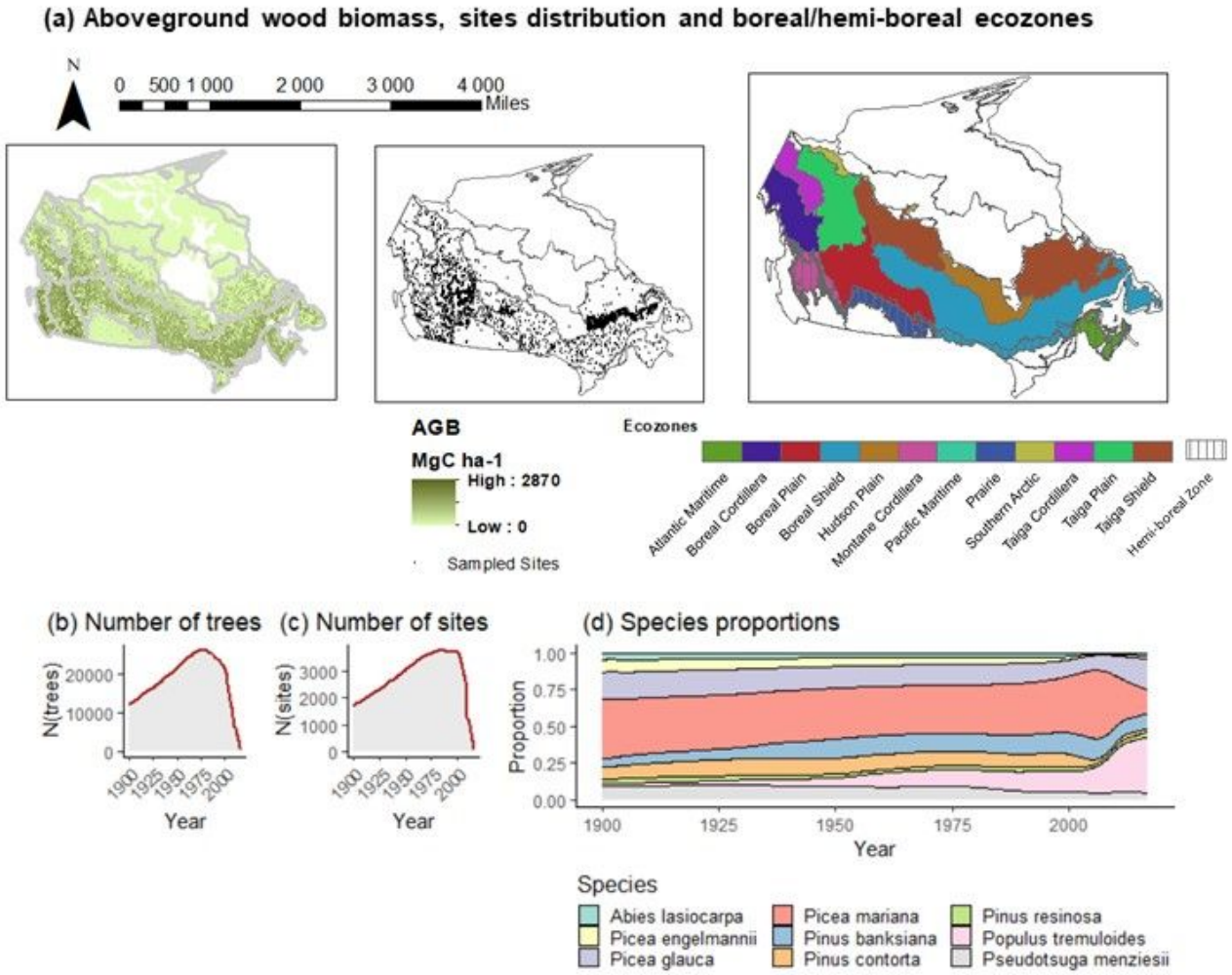

Figure 1

Description of tree-ring dataset. (a) Distribution of sample sites. The background colour on the map at left illustrates the distribution of the aboveground biomass (AGB) across Canada's forests (Spawn & Gibbs, 2020), the distribution of sample sites for the tree-ring dataset encompassing the nine sampled species is represented by points. Canadian Ecoregions are illustrated on the map at right, with the hemi-boreal zone overlaid. Yearly temporal distributions of sampled (b) trees, (c) sites, and (d) species proportions.

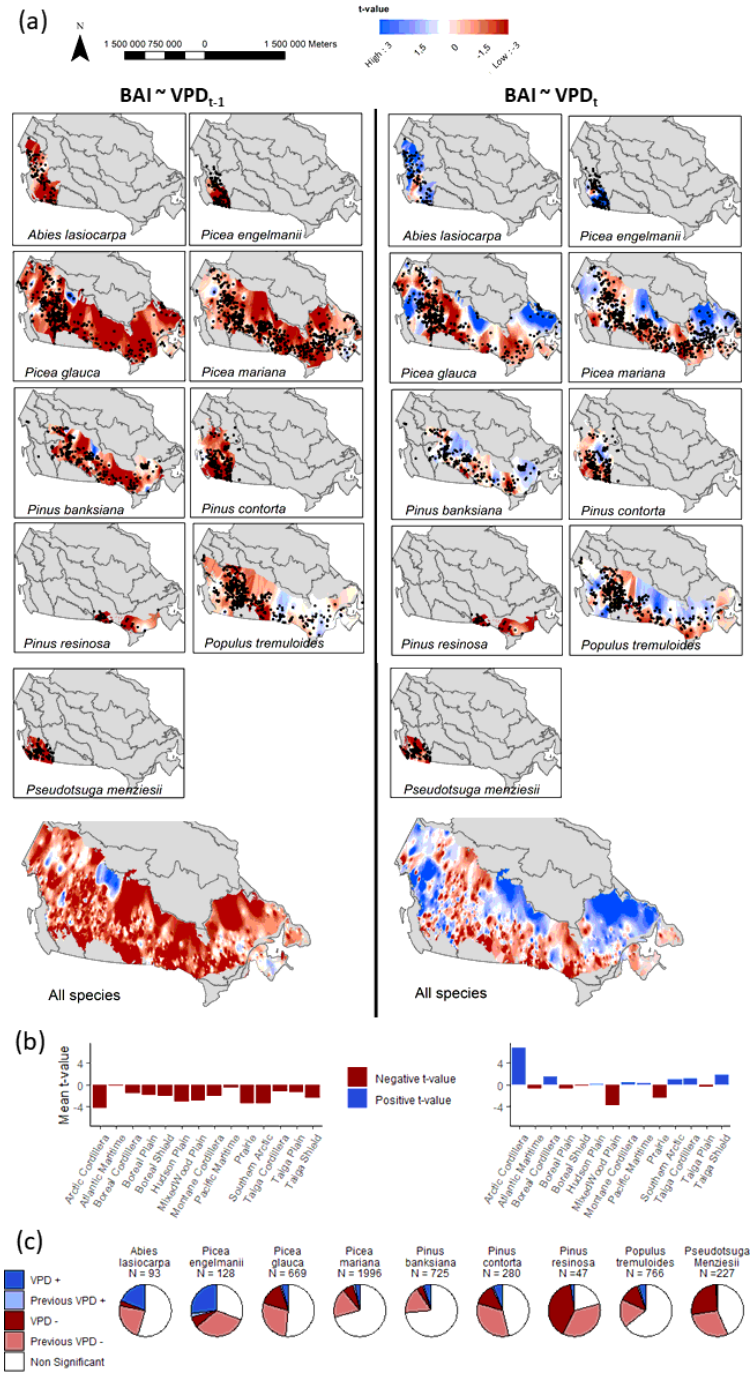

Figure 2

Pointwise *t*-values of the regression between annual growth fluctuations estimated from tree rings (BAI) and vapour pressure deficit (VPD) for the nine tree species. (a) Maps are displaying site-species *t*-values, a bidimensional interpolation was performed on a spatial resolution of 0.1 x 0.1 degree, using the inverse distance weighting method based on the 8 closest neighbours. Interpolations were bounded using boreal mask (all species map) and species distribution area (species maps) (Critchfield & Little, 1966; Little & Viereck, 1971). Below are displayed the (b) means of *t*-values by ecoregions and (c) proportions of non-significant, positive and negative *t*-values for VPD_t and VPD_{t-1}, among convergent models, with the number *N* of corresponding sites.

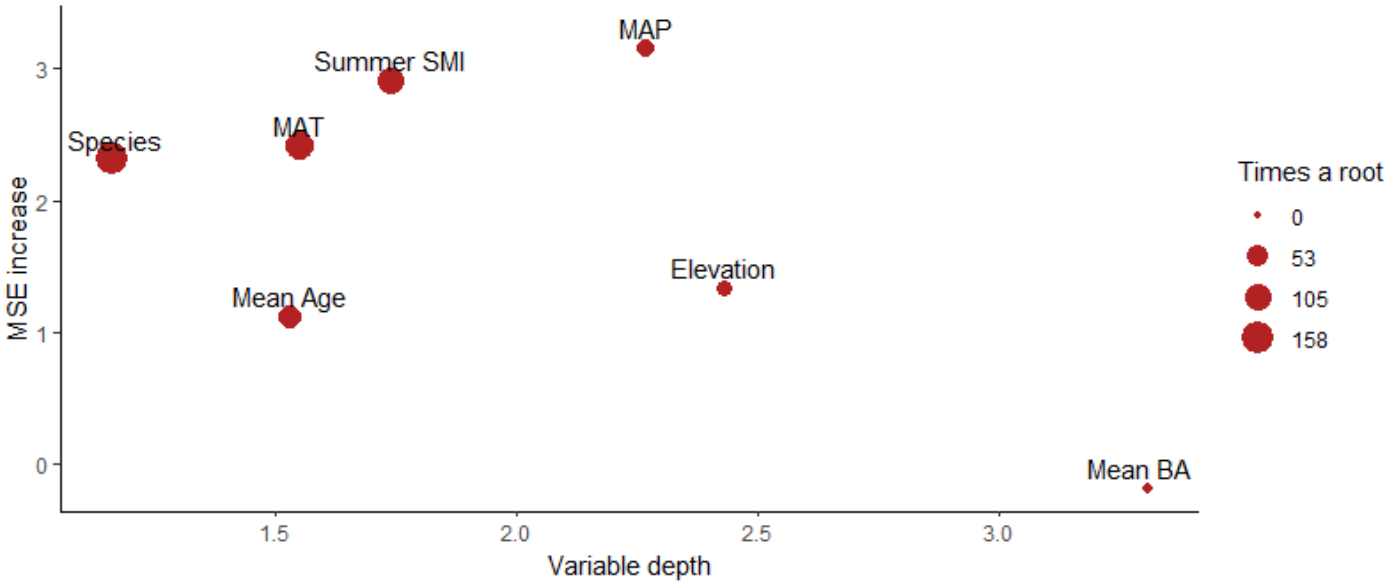

Figure 3

Output of random forest algorithm predicting *t*-values from the seven environmental, tree species and forest structure variables. The x-axis retrieves the variable depth in the tree, and dot size represents variables occurrence as root node (i.e. more frequent root node occurrence equals larger dot); the y-axis retrieves variables' importance, measured as an increase in decision tree mean square error (MSE) when the variable is randomized. Results based on bootstrap with 500 decision trees (also see Table 1).

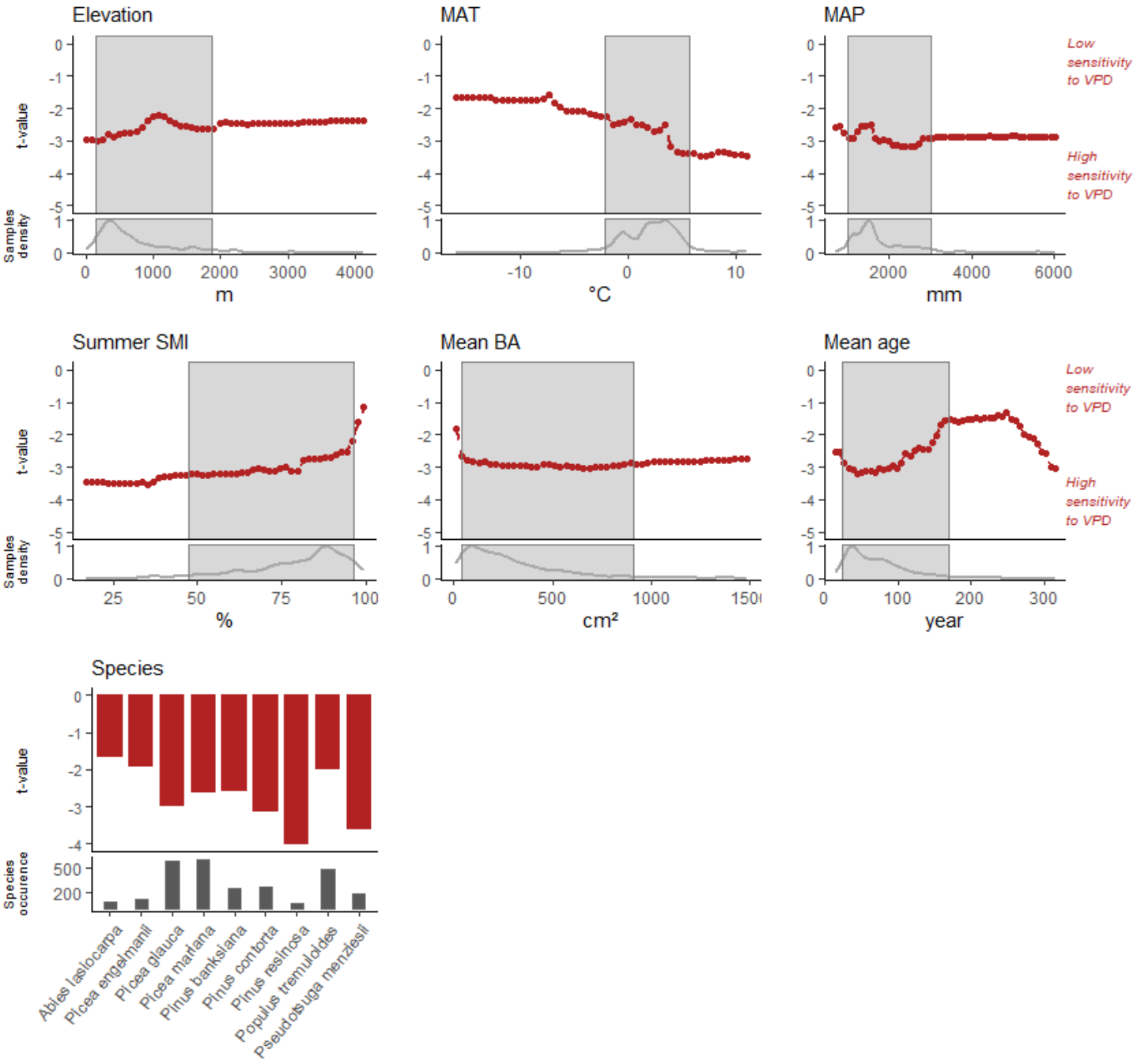

Figure 4

Partial plots of the random forest algorithm showing the marginal effects of six environmental, tree species and forest structure variables on nine species. The y-axis indicates t-value changes predicted by the random forest model in response to changes in the corresponding x-axis variables. The lower curves represent sample density, while the gray shaded area indicates 95% sample coverage. The "Species" figure shows the number of sampled trees per species.

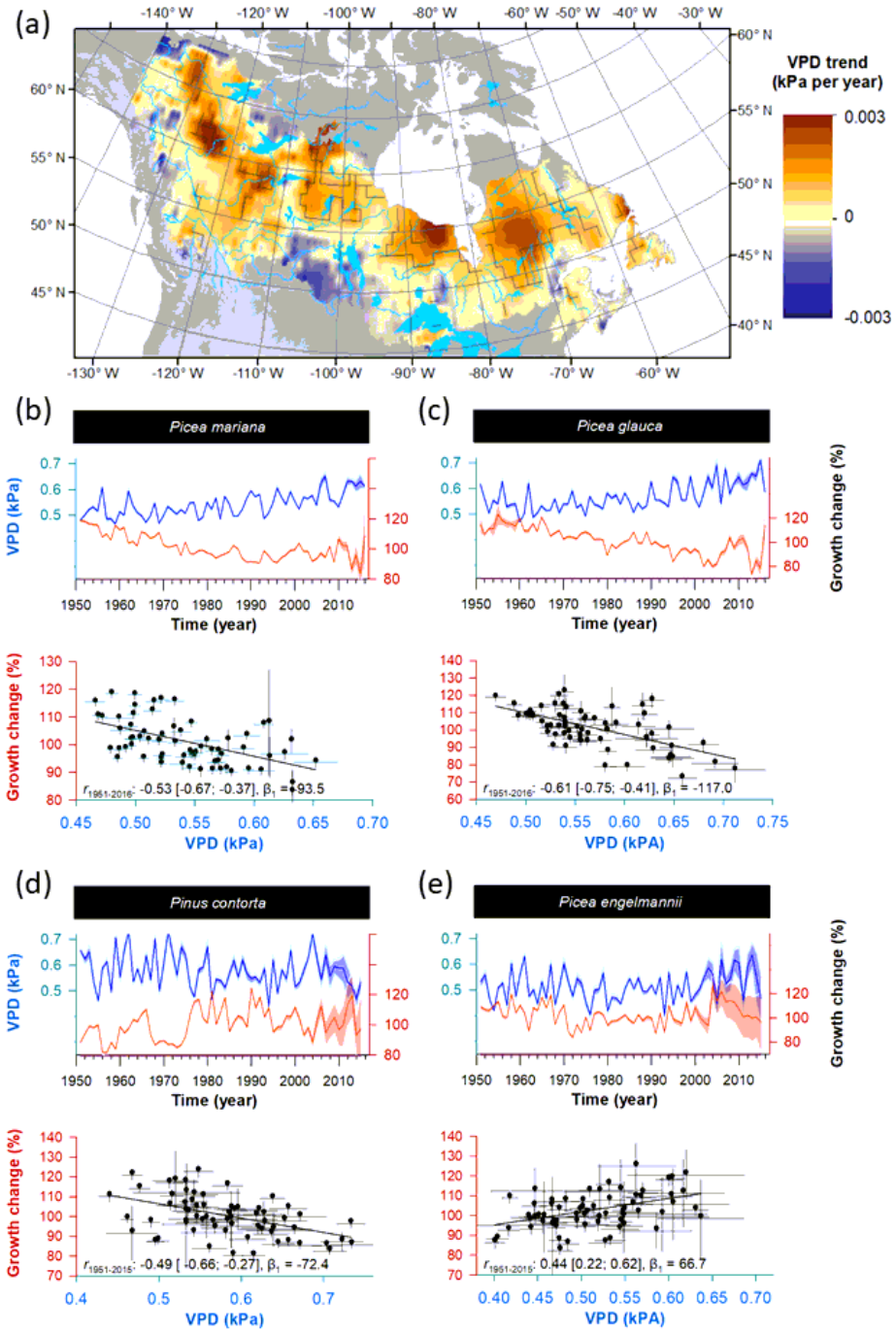

Figure 5

Changes in the annual growth of *Picea mariana, Picea glauca*, *Pinus contorta* and *Picea englemanii* relative to summer VPD. (a) Temporal trends in summer VPD (kPa / year) since 1951. Percent growth change (in red) averaged across all sites relative to (b-d) prior- and (e) current-summer VPD (in blue). Shaded areas represent the 95% confidence interval. Annual growth changes are percent deviation from predicted values generated by the generalized additive mixed models representing the BAI variations unrelated to tree development stage (see Material and methods, eq. 3). Correlative relationships (*r*) between growth changes and summer VPD; the 95% confidence intervals around *r* were computed from a bootstrapping technique that accounted for autocorrelation and trend in data (Mudelsee & Alkio, 2007), and regression slope (β_1) from ordinary-least-square regressions.

Supplementary Files

This is a list of supplementary files associated with this preprint. Click to download.

- Supplementaryinformation.docx